Computers and Concrete, *Vol. 18, No. 6 (2016) 1097-1112*
DOI: http://dx.doi.org/10.12989/cac.2016.18.6.1097

Transient heat transfer analysis using Galerkin finite element method for reinforced concrete slab exposed to high elevated temperature

Byung-Chan Han[1], Young-Jin Kwon[2], Byung-Jae Lee[*3], Seung-Jun Kwon[4] and Young-Suk Chae[5]

[1]*Department of Architectural Engineering, Woosong College, Daejeon 300-715, Korea*
[2]*Department of Emergency Management Engineering, Hoseo University, Chungnam 336-795, Korea*
[3]*R&D Center, JNTINC Co. LTD., Gyeonggi, 18284, Korea*
[4]*Department of Civil and Environmental Engineering, Hannam University, Daejeon 306-791, Korea*
[5]*Department of Architectural Engineering, Woosong University, Daejeon 300-715, Korea*

(Received November 9, 2014, Revised June 26, 2016, Accepted September 12, 2016)

Abstract. Fire loading causes a critical collapse of RC (Reinforced Concrete) Structures since the embedded steels inside are relative week against high elevated temperature. Several numerical frameworks for fire resistance have been proposed, however they have limitations such as unstable convergence and long calculation period. In the work, 2-D nonlinear FE technique is proposed using Galerkin method for RC structures under fire loading. Closed-form element stiffness with a triangular element is adopted and verified with fire test on three RC slabs with different fire loading conditions. Several simulations are also performed considering fire loading conditions, water contents, and cover depth. The proposed numerical technique can handle time-dependent fire loading, convection, radiation, and material properties. The proposed technique can be improved through early-aged concrete behavior like moisture transport which varies with external temperature.

Keywords: fire loading; FE techniques; element stiffness; water content; early-aged concrete behavior

1. Introduction

The high-temperature environment by a fire is considered as one of the ultimate loads in RC(Reinforced Concrete) structure. Since concrete has been recognized as an excellent fire proof construction material, the fire proof performance has been mainly evaluated by simple analysis or by the checkup of guidelines of fire resistance (Harmathy 1993). However, studies of various accident cases reveal the possibility of collapse due to decrease in the effective member section area, damage to steel, and spalling of cover concrete by direct exposure to fire (Kodur 2003, Kwon 2011), so that engineering and social interests are increasing in the fire resistance of concrete. Particularly, experimental and numerical analysis studies are also required for determining reuse of

[*]Corresponding author, E-mail: lbjae80@hanmail.net

http://www.techno-press.org/?journal=cac&subpage=8 ISSN: 1598-8198 (Print), 1598-818X (Online)

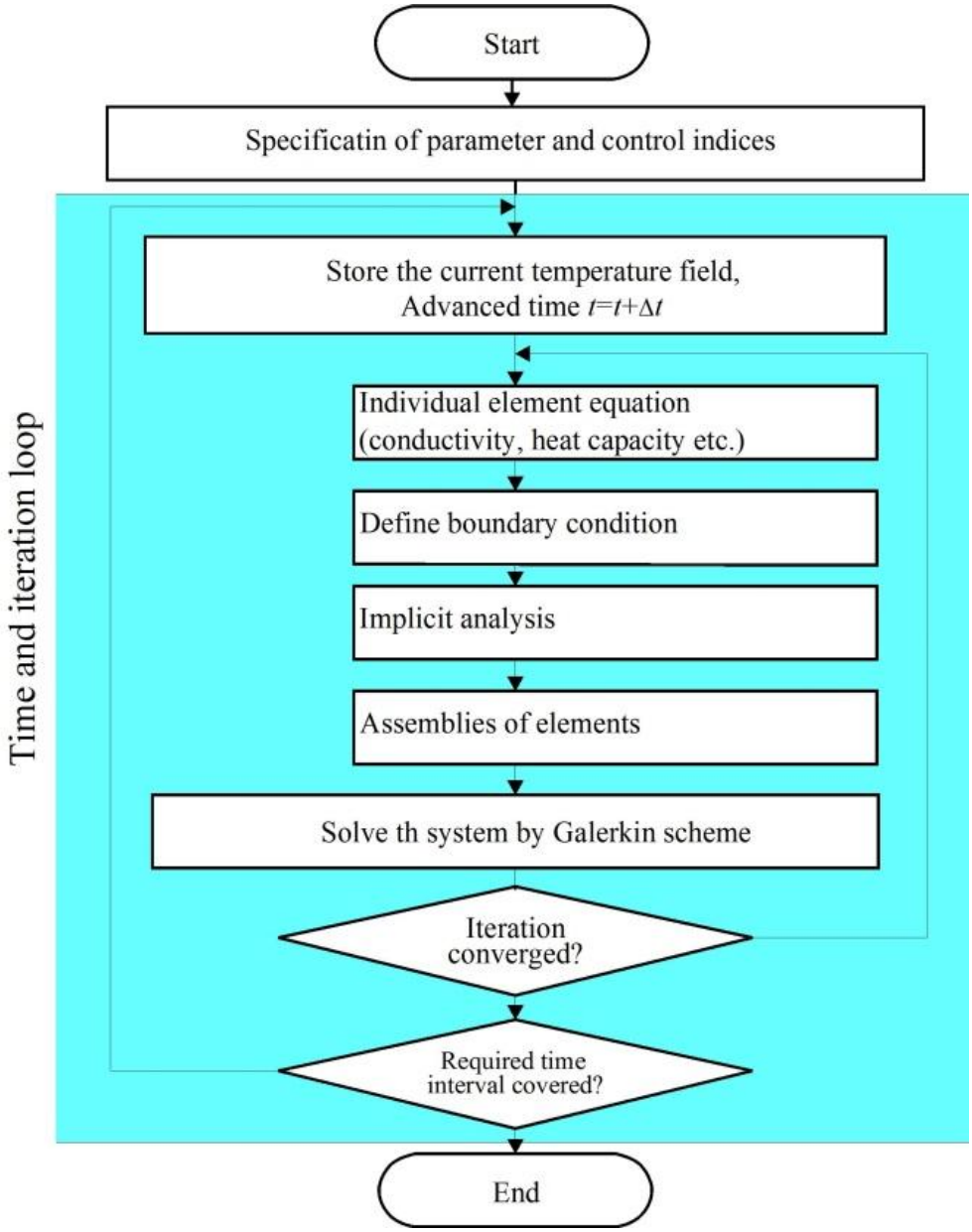

Fig. 1 Flowchart of the proposed algorithm and technique

RC structures which were exposed to fire. Previous researches in Korea have been mainly conducted for the experimental studies on the fire proof performance of unit RC member of a structure or on the macroscopic numerical analysis studies (Shin *et al*. 2011, Kang and Hong 2001). These studies only based on the previous results of the thermal properties of a member and analysis of unit member have limitations in order to evaluate the time-dependent temperature change in a member and local variation of thermal stress.

Several evaluation techniques have been suggested for the fire proof performance in RC members using approximate analytical techniques such as FDM (Finite Difference Method) or FEM(Finite Element Method) (Lee *et al*. 2005, Han *et al*. 2007). The models on heat transfer in concrete based on FDM have problems such as the system stability regarding the analysis of the members with a drastic temperature change, which is caused by the limitations of temperature distribution assumption and the time step convergence condition. Studies employing general-purpose FE analysis software including DIANA are reasonable for practical analysis, but not for research because several limitations are reported such as various types of boundary conditions and temperature-dependent thermal properties of a material (Han *et al*. 2007). Lie (1984) and Kodur (1999) have actively conducted numerical analysis studies on the fire proof performance of concrete. However these studies on the fire proof performance including heat transfer are performed and verified by the test results from individual Codes and Specifications since they require a number of assumptions like governing equations, fire loading, boundary conditions, thermal properties of the materials, the time-temperature dependence relations (Loh *et al*. 2007).

This paper proposes a nonlinear transient heat flow analysis technique using the weighted-residual finite element method, specialize it to the Galerkin method for evaluation for the fire proof performance of RC structure undergoing high-temperature environment. The Galerkin method is limitedly applied to structural analysis in general but mainly employed in a formulation method for partial differential equations handling temperature, fluid, and mechanical problems. The proposed numerical technique is constituted by FORTRAN 90 and the results are verified with test results of 1-side fire resistance test for RC slab member.

Galerkin FEM formulated above is encoded by FORTRAN 90 according to the algorithm shown in Fig. 1. The analysis process employs an explicit scheme which provides the advantage that the stiffness matrix can be simple without manipulation. The applied algorithm is appropriate for a parallel processing environment where several computers are used if necessary, because the calculation is performed independently at each step, and the temperature and time are calculated step by step. In addition, the algorithm is also advantageous in view of the expandability of calculation of the stress caused by elevating temperature since it has the geometric flexibility of FEM. This also provides fast calculation of nodes input and stable convergence. In Fig. 1, the flowchart of the proposed technique is shown.

The temperature-dependent thermal properties of concrete and reinforcing bars from the references (Cho *et al*. 2010), the Guidelines and Specifications (Eurocode 2 1996), and arbitrary experimental results can be considered through user subroutines.

2. Non-Linear temperature distribution analysis

2.1 Governing equation

Governing equation for heat transfer in two-dimensional condition can be written as Eq. (1).

$$\rho(T)C(T)\mathbf{T_t} = (\lambda(T)\mathbf{T_x})_\mathbf{x} + \left(\lambda(T)\mathbf{T_y}\right)_\mathbf{y} \tag{1}$$

where ρ is density (kg/m^3), λ is heat conductivity (W/m.K) C is specific heat (J/kg.K), which are the temperature-dependent thermal properties of the material, and T is temperature (℃).

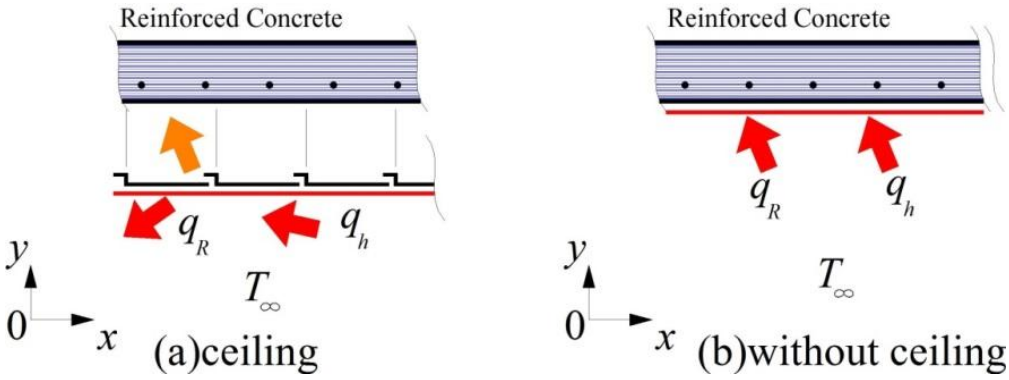

Fig. 2 2-Dimensional conduction with surface convection-Boundary

2.2 Evaluation of boundary conditions considering temperature variation

The entire boundary condition with respect to the surrounding temperature (T_∞) by fire can be shown in Fig. 2. Equivalent heat flux and initial condition are expressed as Eq.(2) and Eq.(3) respectively.

$$-\lambda(T)T_n = q_R + q_h = q_e \tag{2}$$

$$T(x,0) = f(x) \tag{3}$$

where q_R is heat flux by radiation(W/m^2), q_h is heat flux by convention, and q_e is equivalent heat flux. The actual equivalent heat flux (q_e) by gas and ceiling material is considered at the boundary conditions. In the Eq.(2), the heat flux by radiation q_R (W/m^2) is considered as Eq. (4).

$$q_R = \varepsilon\sigma(T_\infty^4 - T_0^4) \tag{4}$$

where σ is Stefan-Boltzmann constant (=5.6697×10^8 W/m^{2}K), ε is surface emissivity, and T_∞ and T_0 are the surrounding air temperature and surface temperatures, respectively. The surface emissivity (ε) is calculated based on Lambert-Bell's Law as Eq.(5).

$$\varepsilon = \frac{i_0 - i}{i_0} = 1 - e^{-k\bar{L}} \tag{5}$$

where i denotes the radiant intensity of the radiation permeable gas(body), k is the absorption coefficient, and $\bar{L}$ means optical path length of the radiation of permeable gas. When gas is accompanied, q_R within a unit zone is written as Eq.(6).

$$q_R = \frac{\varepsilon_1\varepsilon_G\sigma A_G}{1-(1-\varepsilon_1)\left(1-\varepsilon_G\frac{A_G}{A_1}\right)}(T_\infty^4 - T_0^4) \tag{6}$$

where the subscripts 1 and G denote the zone with gas and without gas, respectively. If a

Table 1 Physical properties of air for the analysis

specific heat- c_p (kJ/kg·K)	viscosity coefficient- μ (Pa·s)	dynamic viscosity coefficient- ν (m^2·s)	heat conductivity - λ (kW/m·K)	thermal diffusion coefficient- α (m^2/s)
1.0	$2.5\times10^{-7}T^{3/4}$	$7.2\times10^{-10}T^{7/4}$	$3.7\times10^{-7}T^{3/4}$	$1.0\times10^{-9}T^{7/4}$

space is full of gas (A_G=A_I) and there is a ceiling material before RC slab ($q_{R,L} >> q_{R,U}$), q_R can be written as Eq.(7) and Eq.(8), respectively.

$$q_R = \frac{\varepsilon_1 \varepsilon_G \sigma}{1-(1-\varepsilon_1)(1-\varepsilon_G)}(T_\infty^4 - T_0^4) \tag{7}$$

$$q_R = \frac{q_{R,L} + q_{R,U}}{2} \approx \frac{q_{R,L}}{2} \tag{8}$$

where the subscripts L and U denote the space under and above the ceiling, respectively.
According to the Newton's law of cooling, the heat flux by convection (q_h) is calculated as Eq. (9).

$$q_h = h(T_\infty - T_0) \tag{9}$$

where h is convection coefficient (W/m^2℃). Since a fire is heat transfer by forced convention and turbulence, the mean Nusselt number N_U is considered as Eq.(10) and Eq. (11).

$$\mathrm{h} = \frac{\lambda}{L} N_u \tag{10}$$

$$N_u = 0.037 Pr^{1/3} Re_x^{4/5} \text{ (turbulent flow)} \tag{11}$$

where the *Pr* is Prandtl number (= *ν*/*α* = 0.72), and $\mathrm{Re}_x = qL/\nu$, where q is air heat flux. Physical properties of the air are summarized in Table 1. If there is a shield such as ceiling, q_h can be assumed as 0.

Considering Eq.(4) and (9), Eq.(2) can be shown in Eq.(12) .

$$q_e = (h + \alpha_R)(T_\infty - T_0) \tag{12}$$

where $\alpha_R = \varepsilon\sigma(T_\infty^2 + T_0^2)(T_\infty + T_0)$, and T_0 denotes the surface temperature calculated at time t_n.

2.3 Formulation of Galerkin FEM (*Harada 1992*)

Mesh generation is carried out using three-node triangular elements as shown in Fig. 2 and then FEM is formulated by the Galerkin method (Harada 1992). In Fig. 3, if the temperature at each node in an element is assumed to be T_i^e (i=1,2, and 3), it is constructed as $\{T^e\}$ in matrix formation.

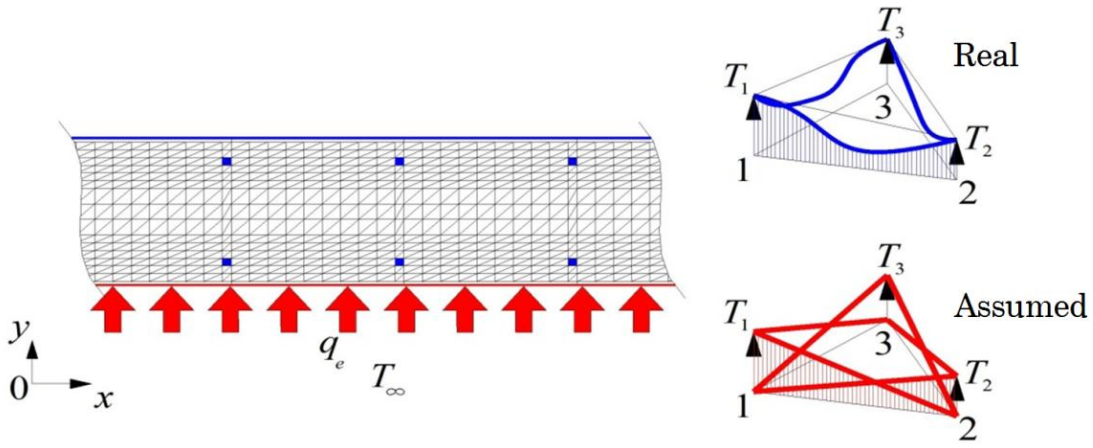

Fig. 3 Triangular element and temperature transfer with shape function

Simplifying with a shape function (N_i), it can be formulated as Eq.(13).

$$T^e(x,y) = \sum_{i=1}^{3} N_i\, T_i^e \tag{13}$$

From Eq. (1), the residual *R* can be formulated as Eq.(14).

$$\mathrm{R} = (\lambda(\mathrm{T})\mathbf{T_x})_\mathbf{x} + \left(\lambda(\mathrm{T})\mathbf{T_y}\right)_\mathbf{y} - \rho(T)C(T)\mathbf{T_t} \tag{14}$$

Assuming $\rho(T)$, $\lambda(T)$, and $C(T)$ are constant at an arbitrary temperature in an element, Eq.(14) is rewritten as Eq.(15).

$$\mathrm{R} = \lambda\left(\mathbf{T_{xx}} + \mathbf{T_{yy}}\right) - \rho C\mathbf{T_t} \tag{15}$$

Considering N_1 as a weight function, Eq.(16) can be obtained and this can be rewritten as Eq.(17) for substituting Eq.(13).

$$\iint_\Omega N_1 R d\Omega = \iint_\Omega N_1\left[\lambda\left(\mathbf{T_{xx}} + \mathbf{T_{yy}}\right) - \rho C\mathbf{T_t}\right]d\Omega = 0 \tag{16}$$

$$\sum_{i=1}^{3}\left[\lambda \iint_\Omega N_1\left\{(\mathbf{N}_i)_{\mathbf{xx}}+(\mathbf{N}_i)_{\mathbf{yy}}\right\}d\Omega T_i^e\right] - \sum_{i=1}^{3}\left[\rho C \iint_\Omega N_1 N_i d\Omega (\mathbf{T}_i^e)_\mathbf{t}\right] = 0 \tag{17}$$

Expanding the first term of Eq.(17) by Green-Gauss theorem, Eq.(18) can be obtained, where $\int_\Gamma N_1 (N_i)_n d\Gamma$ denotes the linear integration with respect to the element boundary. Eq.(18) is considered in Eq.(17), which yields Eq.(19).

$$\iint_\Omega N_1\left\{(\mathbf{N}_i)_{\mathbf{xx}}+(\mathbf{N}_i)_{\mathbf{yy}}\right\}d\Omega = -\iint_\Omega \left\{(\mathbf{N_1})_\mathbf{x}(\mathbf{N}_i)_\mathbf{x} + (\mathbf{N_1})_\mathbf{y}(\mathbf{N}_i)_\mathbf{y}\right\}d\Omega - \int_\Gamma N_1(\mathbf{N}_i)_\mathbf{n} d\Gamma \tag{18}$$

$$\sum_{i=1}^{3}\left[\lambda\iint_{\Omega}\{(\mathbf{N}_1)_{\mathbf{x}}(\mathbf{N}_i)_{\mathbf{x}}+(\mathbf{N}_1)_{\mathbf{y}}(\mathbf{N}_i)_{\mathbf{y}}\}d\Omega\,T_i^e\right]+\sum_{i=1}^{3}\left[\lambda\int_{\Gamma}N_1(\mathbf{N}_i)_{\mathbf{n}}d\Gamma\,T_i^e\right]+\sum_{i=1}^{3}\left[\rho C\iint_{\Omega}N_1N_i d\Omega\,(\mathbf{T}_i^e)_{\mathbf{t}}\right]=0 \tag{19}$$

Here, the second term in Eq.(19) can be expressed as Eq.(20).

$$\sum_{i=1}^{3}\left[\lambda\int_{\Gamma}N_1(\mathbf{N}_i)_{\mathbf{n}}d\Gamma\,T_i^e\right]=\int_{\Gamma}N_1(\lambda(\mathbf{T}_i^e)_{\mathbf{n}})d\Gamma \tag{20}$$

Since the boundary condition in Eq.(2) can be substituted as the temperature gradient, when the element boundary is an external boundary, Eq.(20) can be written as Eq.(21). This also yields Eq.(22) considering Eq.(19)

$$\sum_{i=1}^{3}\left[\lambda\int_{\Gamma}N_1(\mathbf{N}_i)_{\mathbf{n}}d\Gamma\,T_i^e\right]=-\int_{\Gamma}N_1(q_eT_\infty)d\Gamma+\sum_{i=1}^{3}\left[\int_{\Gamma}\{N_1N_i d\Gamma\}\,T_i^e\right] \tag{21}$$

$$\sum_{i=1}^{3}\left[\lambda\iint_{\Omega}\{(\mathbf{N}_1)_{\mathbf{x}}(\mathbf{N}_i)_{\mathbf{x}}+(\mathbf{N}_1)_{\mathbf{y}}(\mathbf{N}_i)_{\mathbf{y}}\}d\Omega\,T_i^e\right]+\sum_{i=1}^{3}\left[\int_{\Gamma}N_1N_i d\Gamma\,T_i^e\right]+\sum_{i=1}^{3}\left[\rho C\iint_{\Omega}N_1N_i d\Omega\,(\mathbf{T}_i^e)_{\mathbf{t}}\right]=\int_{\Gamma}N_1(q_eT_\infty)d\Gamma \tag{22}$$

In the same manner with respect to N_2 and N_3, governing equation in one element can be constructed as Eq.(23) in the matrix form.

$$\left[\rho C\iint_{\Omega}N_iN_j d\Omega\right](\mathbf{T}_i^e)_{\mathbf{t}}+\left[\lambda\iint_{\Omega}\{(\mathbf{N}_1)_{\mathrm{x}}(\mathbf{N}_i)_{\mathbf{x}}+(\mathbf{N}_1)_{\mathbf{y}}(\mathbf{N}_i)_{\mathbf{y}}\}d\Omega+\int_{\Gamma}N_iN_j d\Gamma\right]\{T_i^e\}=\left\{\int_{\Gamma}N_i\{q_eT_\infty\}d\Gamma\right\} \tag{23}$$

2.3 Construction of the global equation and time integral

Constructing the equation after calculating the individual element equations of Eq.(23) for each element, global equation can be constructed as Eq. (24).

$$[\mathrm{C}]T_t+[G]\{T\}=\{B\} \tag{24}$$

Where, $[\mathrm{C}]$, T_t $[G]$, $\{T\}$ and $\{B\}$ is global matrix in the each term of Eq.(23)

Table 2 Specimens prepared for the fire test

Specimen	Heating rate	Heating time (min)
ISO-120	ISO 834, Eq (27)	120
ARB-60	Arbitrary, Eq (28)	60
ARB-120	Arbitrary, Eq (28)	120

Table 3 Concrete mix proportions and material properties

f_c (MPa)	W/B (%)	Air	FA/B (wt.)	Unit weight (kg/m^3)					
				W	C	FA	SF	Sand	Gravel
30	60	4	0.10	168	244	28	8	750	1014
Compressive strength of concrete (MPa)				Yield strength of rebar (MPa)				Moisture content of concrete (%)	
31.0				410.0				4.9	

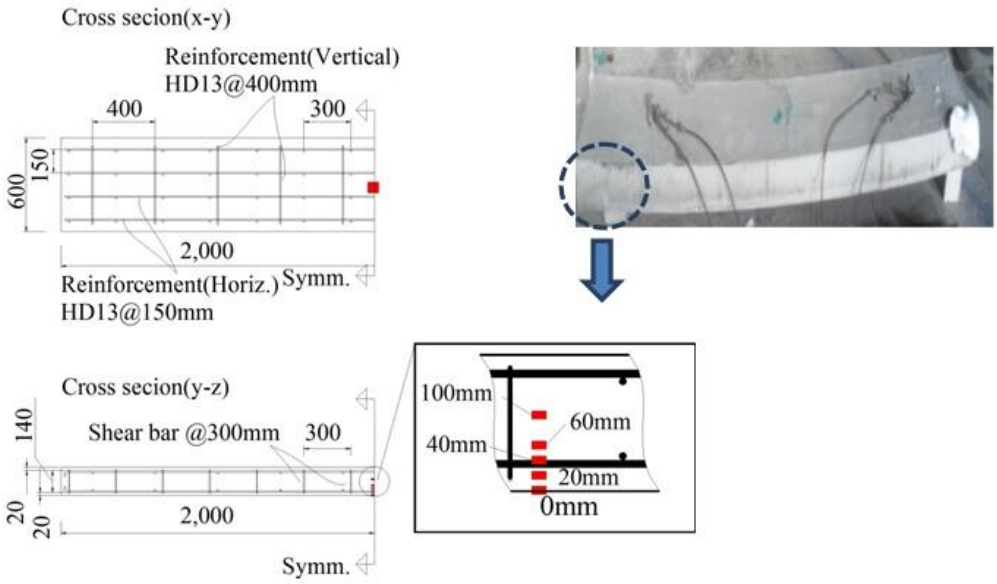

Fig. 4 Geometry and details of specimen and sensor installation

In the differential of Eq.(24) with respect to time (t) is written as Eq.(25).

$$\{\mathbf{T_t}\} = \frac{1}{\Delta t}[\{T^{n+1}\} - \{T^n\}],\ \{T\}^n = \left\{T_{(t=n\Delta T)}\right\},\ \{T\} = \{T^{n+1}\} \tag{25}$$

where n denotes the time step. Therefore Eq.(24) can be expressed as Eq.(26) using Eq.(25) with time step.

$$\left[\frac{[C]}{\Delta t} + [G]\right]\{T^{n+1}\} = \frac{[C]}{\Delta t}\{T^n\} + \{B\} \tag{26}$$

The temperature at each node can be obtained using Eq. (26).

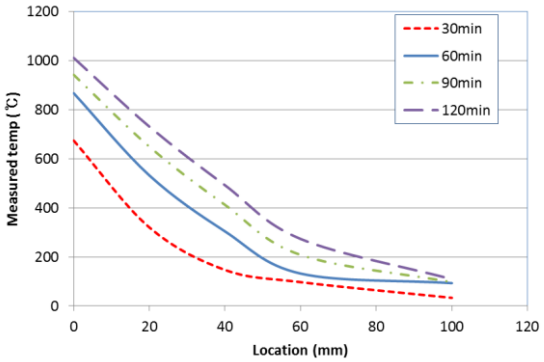

(a) specimen ISO-120

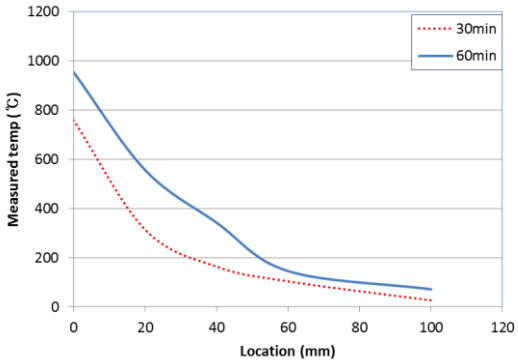

(b) specimen ARB-60

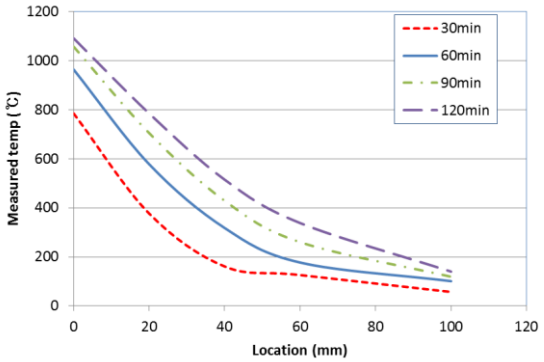

(c) specimen ARB-120

Fig. 5 Temperature profiles measured from fire tests

3. Tests verification of the proposed numerical analysis

3.1 Experimental program

To verify the validity of the proposed technique handling transient temperature distribution analysis by Galerkin FEM, fire resistance tests of RC slab are performed. Three specimens are

prepared considering the heating load size and the heating time as the key variables, as shown in Table 2. The specimens are unidirectional RC slabs of 600×180×4000 mm size, and four reinforcing bars are arranged at the top and at the bottom with the cover depth of 20 mm referred to the previous test (Cho *et al*. 2010). Concrete mix proportions and engineering properties are listed in Table 3. Thermocouples are installed in the center of the specimens at the positions of 0, 20, 40, 60, and 100 mm from the heated surface (bottom), which is shown in Fig. 4 with geometry and thermocouple installation.

Fire resistance test is carried out at the Fire Insurers Laboratories of Korea. The specimens are located at simple support in a horizontal furnace and one surface is heated with heating area of 600×180×3700mm. The test is performed on specimen ISO-120 based on the ISO 834 in Eq.(27). The tests on ARB-60 and ARB-120 are performed considering arbitrarily increasing fire load like Eq. (28).

$$T_{\infty} = 345\log(8t + 1) + 20 \tag{27}$$

$$T_{\infty} = 510t^{1/6} + 20 \tag{28}$$

where t denotes time (minute)

3.2 Experimental results

Deflections in the specimens are observed after heating, and maximum deflection is up to 100 mm in the ISO-120 specimen. All the specimens show partial spalling due to elevating temperature but it does not happen at the position of sensor location. More severe spallings are observed in the specimens ARB-60 and ARB-120, which have a larger fire loading than the ISO-120 specimen for verification of the proposed work. The measured temperature profiles for each specimen are plotted in Fig. 5. The temperature on the heated surface (0 mm) is different from the heating curve in all the specimens due to the convention effect. In the interval of temperature raising between 100~150 ℃, the gradient of the temperature is evaluated to be smaller due to the effect of the internal pore water. The maximum temperature at the position of the reinforcing bar (20 mm) is approximately 731 ℃, 556 ℃ and 785℃ in the ISO-120, ARB-60, and ARB-120 specimens, respectively.

4. Verification of the proposed numerical analysis

4.1 Modeling for the verification of the proposed method

4.1.1 Consideration of the boundary conditions

The proposed technique of temperature distribution analysis is verified with the test results. The modeling and analysis are performed considering the symmetry of the specimen with the three-node triangular elements. In the boundary region, the elements are discritized into half size with reference to 20×20mm considering the drastic temperature gradient. In the test, the size of the furnace is 4.3×3×1.6m, the surface area (A) is 46.4 m^2, so that the mean radiant temperature($\bar{L}$) is 1.49m (3.6 V/A). Diesel is used for heating so k is determined as $0.43m^{-1}$ (not standard parameter), which is considered in Eq. (5), this yields Eq. (29).

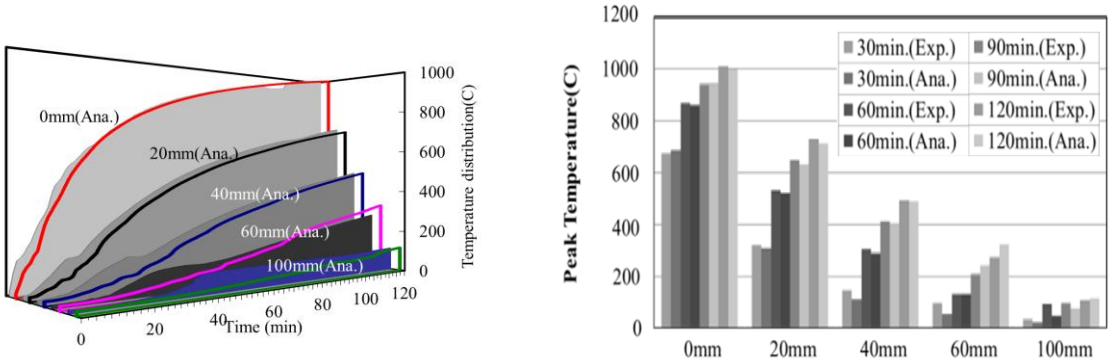

(a) specimen ISO-120

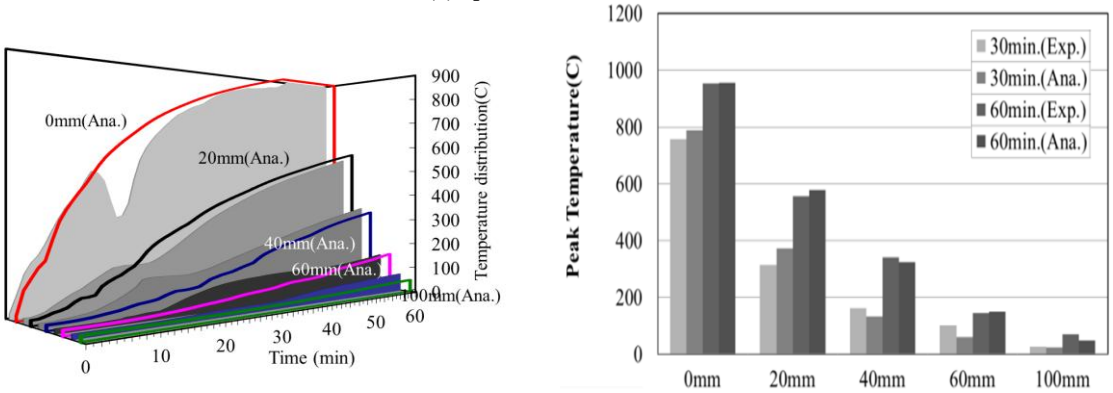

(b) specimen ARB-60

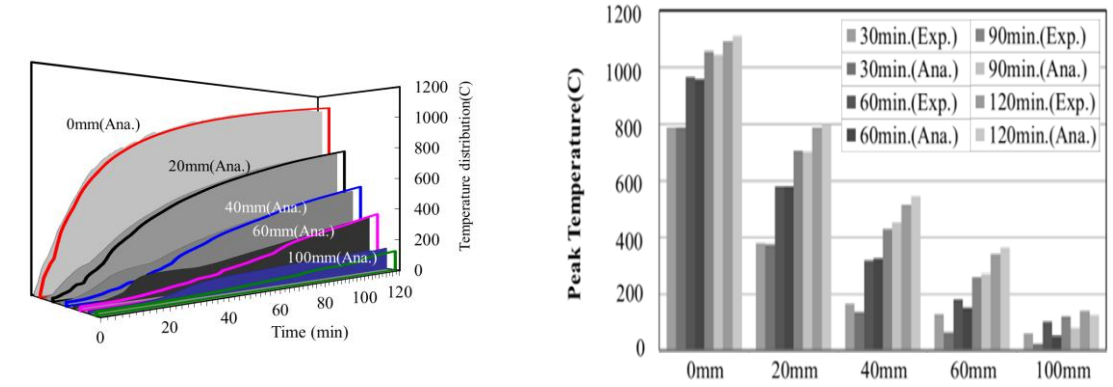

(c) specimen ARB-120

Fig. 6 Comparison between measured and simulated temperature

$$\varepsilon = 1 - e^{-k\bar{L}} = 0.4731 \tag{29}$$

Assuming forced convection and the turbulence flow velocity (u_∞=8 m/s), in which heat flux is parallel with the heated surface, the ranges of Re_x and h are 3×10^5~ 3×10^6 and 13.4~33.3 from Eq. (10) and Eq. (11).

4.1.2 Thermal properties of material

The thermal properties for concrete (λ_C , $\rho_C C_C(t)$) and steel (λ_S $\rho_S C_S$) are assumed referred to the previous work (Cho *et al*. 2010), which are listed in Eq.(30)~(33).

$$\lambda_c(t) = \begin{cases} \xi[1.5 - (0.5/800)T] & (\lambda > 1.0) \\ \xi & (\lambda < 1.0) \end{cases} \tag{30}$$

$$\lambda_s = 40 \tag{31}$$

$$\rho_C C_C(t) = \begin{cases} \rho_C(930) & (T < 90) \\ \rho_C(930) + \rho_C w_t \dfrac{(590 \times 4190)}{20} & (90 \le T < 110) \\ \rho_C(930) & (T \ge 110) \end{cases} \tag{32}$$

$$\rho_s C_s = 7850(482) \tag{33}$$

In Eq. (44), parameter ξ (0.80) is added for effect on heat conduction and w_t are set as 4.9% based on the test result.

4.2 Numerical analysis results and verification

The test results are compared with simulated results in Fig. 6. Fig. 6 shows that the proposed technique is evaluated to reasonably simulate the temperature hysteresis of test results. Particularly, the proposed technique provides very accurate results within 10% of relative errors at the steel location (20 mm) at each heating time (30 min, 60 min, 90 min, and 120 min) except for ARB-60 specimen at 30 minutes. However, the relative error gradually increases as increasing cover depth from the heated surface. The maximum prediction error in terms of the ratio of numerical analysis result to the experimental result is approximately 0.50 at the 100 mm position from the heated surface. The reason for the big error is thought to be:

1] No consideration of the retardation of the temperature gradient by the water transport or latent heat.

2] Relatively small input value of equivalent convection coefficient.

3] Experimental error (overheating of test).

4] Accumulation of errors in the small difference. Nevertheless, the estimated temperature hysteresis is in a good agreement with the actual test data and the simulated temperature distribution at the steel location is very accurate.

5. Simulation of parameter effect

In order to analyze the effect of each parameter on the temperature distribution, several simulations using the proposed technique for transient condition are carried out. The key parameters are considered as the size of fire loadings, the thermal properties of the concrete, and the moisture content. The same mesh generation with triangular is adopted and temperatures at two different cover depths (20 and 40mm) are evaluated.

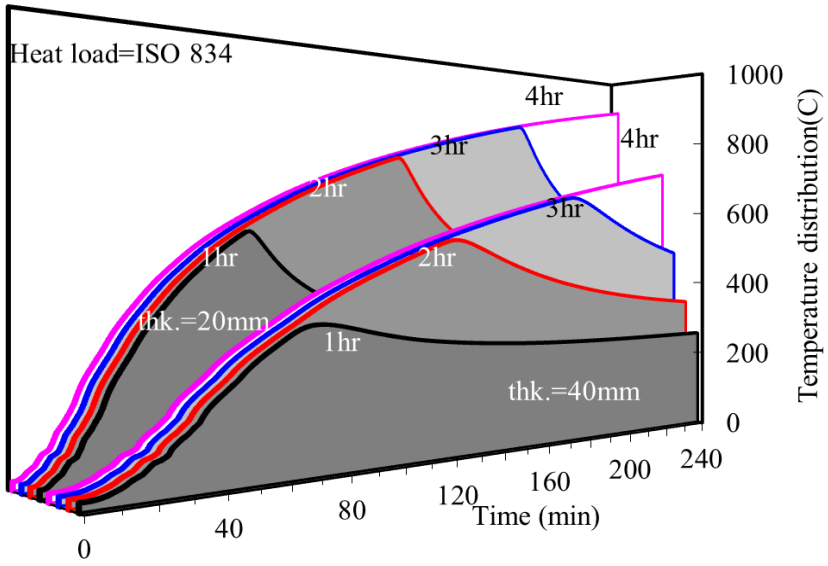

Fig. 7 Effects of heating rate and duration time (ISO 834)

5.1 Effect of the fire loading size (Heating rate and duration time)

The results of the temperature distribution analysis using the standard fire heating curve (ISO 834) at each time (1, 2, 3, and 4 hours) are shown in Fig. 7, where moisture content of 3% and concrete thermal properties in Eq.(44)~ Eq.(47) are assumed. The cooling profile after the heating in Fig.7 is listed in Eq. (34).

$$T_{\infty} = [345\log(8t+1)+20] - \eta[\{345\log 8(t-t_{max})+1\}+20] \tag{34}$$

where $t_{\max}$ is reference heating time and η is assumed as 4.5/3.2 [9].

The simulated result is 729 ℃ at the position of the slab (steel location of 20 mm) by the fire scale of ISO 834 for two hours and 641 ℃ at the position of the column (steel location of 40 mm) by the fire scale of ISO 834 for three hours, which indicates that the target structure does not satisfy the required fire proof performance (538 ℃) (Korean code 2008). Actually, a lower temperature can be expected in a real RC structure by the effect of the gas radiation absorption and the convection, but additional plans for fire resistance (e.g., increased cover depth) are needed to satisfy the required fire poof performance.

5.2 Effect of the thermal properties of the concrete

The effect of the thermal properties of the concrete (moisture content=3%, ISO 834, 2 hours) is shown in Fig. 8. The results based on the thermal properties in Eurocode 2 (1996) are evaluated to be 9~10% lower than those based on the previous research (kwon *et al*. 2010). The reason is that the used thermal properties of the previous work (kwon *et al*. 2010) are higher than those in Eorocode (1996). The difference of the thermal properties is caused by insufficient test results and

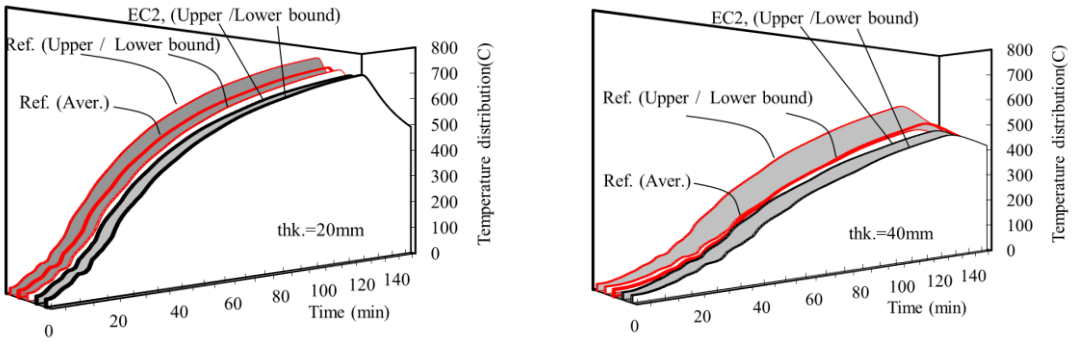

(a) Cover depth 20mm (b) Cover depth 40mm

Fig. 8 Effects of thermal properties in concrete

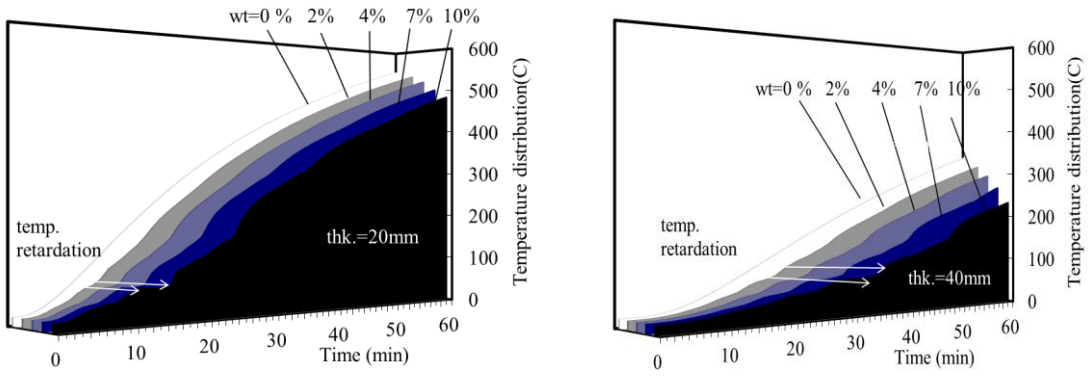

(a) Cover depth 20mm (b) Cover depth 40mm

Fig. 9 Effects of water content

uncertainties of concrete material so that it is necessary to accumulate the experimental data of the concrete thermal properties.

5.3 Effect of the moisture content in the concrete

The effects of the moisture content in the concrete (ISO 834, 2 hour) are shown in Fig. 9. From the analysis, the internal temperature decreases with larger moisture content. In particular, the numerical analysis results reasonably depict the decreasing gradient of the temperature due to the phase change (from liquid to vapor) of the internal water in the range of 90~110℃. The numerical analysis result is slightly different from the actual test result because the moisture transport toward to the inside of concrete and the accelerated evaporation rate due to the transport are not taken into consideration in the proposed technique. However, the proposed technique is practical advantages like fast running time and handling of big data since the currently available numerical methods considering heat and moisture transport are applicable only to the analysis of single member in a

small-scale due to long running time and insufficient divergence.

6. Conclusions

This study is performed as a part of the numerical analysis work on the fire proof performance of RC structure undergoing high-temperature environment such as fire. Through the nonlinear transient heat flow analysis technique using Galerkin FEM, following conclusions are obtained.

1) The verification of the proposed technique with nonlinear transient heat flow analysis using Galerkin method is performed, which shows that the temperature hysteresis is in agreement with the test results with stable convergence and fast calculation. In particular, this technique reasonably simulates the temperature distribution at the steel location. The proposed technique also enables to consider various fire scales, convection/radiation boundary conditions, and the temperature-dependent thermal properties.

2) From the analysis, moisture content is evaluated to relieve the temperature rise gradient. Considering the result, fire damages can be simulated more accurately through an appropriate evaluation of moisture content.

3) The boundary conditions considering heat convection, radiation properties, and temperature-dependency can enable a simulation of the heat transfer characteristics of a RC member to be more close to the test results. In the paper the equivalent convection coefficient (h) and the internal absorptivity of the furnace (ε) are evaluated to be reasonably assumed as 23 and 0.4~0.5, respectively.

4) The proposed technique handling nonlinear transient heat flow does not consider the moisture transport and the evaporation rate accelerated by the transport. More test results need to be accumulated in the future with respect to the analysis of spalling by pore pressure, the interpretation of mass transfer and stress distribution in the case of cracking due to temperature stress, and the thermal properties determination.

Acknowledgements

This research was supported by Basic Science Research Program through the National Research Foundation of Korea (NRF) funded by the Ministry of Science, ICT & Future Planning (No. 2015R1A5A1037548)

References

Cho, C.G., Han, B.C., Lee, J.H. and Kim, Y.Y. (2010), "Flexural test on composite deck slab produced with Extruded ECC Panel", *J. Korea Concrete Inst.*, **22**(5), 695-702.

Eurocode 2 (1996), Design of Concrete Structures Part 1, 2 General Rules-Structural Fire Design, DO ENV 1992.

Han, B.C., Kwon, Y.J., Kim, J.H., Shin, Y.S. and Choi, E.G. (2007), "Temperature-dependency thermal properties and transient thermal analysis of structural frames exposed to fire", *J. Korea Concrete Inst.*, **19**(3), 283-292.

Harada, K. (1992), "A study on the prediction of temperature rise of concrete in fire-resistance Test", Ph.D

Thesis, Kyoto University. Kyoto.
Harmathy, T.Z. (1993), Fire Safety Design and Concrete, Longman Scientific and Technical, Longman House, Burnt Mill, Harlow, ESSEX CM20 2JE, UK..
Kang, S.W. and Hong, S.G. (2001), "Material model and thermal response analysis of concrete at elevated temperatures", *J. Korea Concrete Inst.*, **13**(3), 268-276.
Kodur, V. (2003), "World trade centre disaster-building performance investigation," CSCE workshop at Toronto, 1-18.
Kodur, V.K.R. (1999), "Fire performance of high-strength concrete structural members", Construction Technology Update No. 31, Institute for Research in Construction, National Research Council of Canada, 1-20.
Korean code, 334 (2008), Recommendation on the fire resistance of high-strength concrete beam and column, MOLIT-334, 3-6.
Kwon, Y.J. (2011), Case study damaged by fire and repair methods for concrete building, *Mag. Korea Concrete Inst.*, **23**(3), 44-46.
Kwon, Y.J., Kim, N.H., Lee, J.Y., Kim, D.J. and Harada K. (2010), "Temperature dependency thermal properties of high strength concrete," *Proceedings of Fire Science and Engineering in Japan Association*, 282-283.
Lee, C., Shin, Y.S., Lee, S.W. and Lee, C.E. (2005), "Numerical modeling of heat transfer in reinforced concrete columns exposed to fire", *J. Korea Concrete Inst.*, **17**(6), 871-878.
Lie, T.T., Lin, T.D., Allen, D.E. and Abrams, M.S. (1984), "Fire resistance of reinforce concrete columns", National Research Council Canada Division of Building Research, No. 1167, Ottawa, 25-45.
Loh, J.S., Azid, I.A., Seetharamu, K.N. and Quadir, G.A. (2007), "Fast transient thermal analysis of Fourier and non-Fourier heat conduction", *Int. J. Heat and Mass Transfer*, **50**(21), 4400-4408.
Shin, Y.S., Park, J.E., Mun, J.Y. and Kim, H.S. (2011), "Experimental studies on the effect of various design parameters on thermal behaviors of high strength concrete columns under high temperatures", *J. Korea Concrete Inst.*, **23**(3), 377-384.

CC